Fine Analysis of the Behavior of a Reverberation Chamber in the Frequency Domain with a Model Based Upon Image Theory

Emmanuel Amador, Christophe Lemoine, Philippe Besnier
Université Européenne de Bretagne
INSA, IETR, UMR CNRS 6164
Rennes, France
Email: emmanuel.amador@insa-rennes.fr

Alexandre Laisné
Centre d'essais aéronautiques de Toulouse (CEAT)
DGA-ATU
Balma, France
Email: alexandre.laisne@dga.defense.gouv.fr

***Abstract*—In this article, we propose a model based upon image theory (IT). This very straightforward model designed initially as a time domain model carry the physics of a reverberation chamber (RC) and is able to simulate its behavior in the frequency domain. Simulation results obtained with this model are compared with measurements in the reverberation chamber of our laboratory and an electric field imbalance observed in our reverberation chamber is reproduced with our model.**

I. Introduction

The model presented in this article was initially thought as a time domain model to simulate the behavior of a reverberation chamber (RC) in presence of radar-like signals. With few precautions however, this very straightforward model based on image theory (IT) can be used to simulate an RC in the frequency domain. This paper is dedicated to the exploitation of this model in the frequency domain. Among models available to simulate the behavior of an RC in the frequency domain, the simplest model is certainly the plane-wave model proposed by Hill [1]. It simulates the stochastic nature of the E-field in the chamber but does not integrate the physical dimensions nor the loss in the cavity. More complex models based on transmission line matrix (TLM) techniques [2] or (finite-difference time-domain) FDTD [3], [4], [5], allow to simulate the physics of the chamber through its dimensions and the conductivity of the walls. The spatial discretization of an highly conductive environment induces severe limitations and these models need a lot of attention to simulate an RC efficiently. The model presented in this article is based on IT, it doesn't involve any spatial discretization of the RC nor a discretization of Maxwell's equations. It can be regarded as the simplest model of a reverberation chamber that carries the physics of the cavity without being deterministic. After a quick presentation of the model developed, the behavior of the model is analyzed through the statistics of the E-field and compared with measurement made in our RC at the Institute of Electronics and Telecommunications of Rennes (IETR). In the last section the model is used to explain measurements that show an imbalance of the rectangular components of the E-field in our RC.

II. Model of a Reverberation Chamber with Image Theory

A. Cavity Modeling with Image Theory

The idea of using IT to simulate an RC came with a description of a waveguide by IT in [6]. The RC can easily be represented by a waveguide with two additional boundary conditions. IT was already used to model shielded cavities [7], but the application of this technique is reduced to an asymptotic extraction of the quality factor of the cavity. To our knowledge it is the first paper about a time-domain analysis of a shielded cavity based upon an optical model. Another paper [8] investigates various approaches to model a reverberation chamber. A 2D and a 3D model based on IT are proposed, but the

computer resources did not allow to get relevant results in the frequency domain.

B. Presentation of our model

IT is an optical approach, the construction of the images is based on geometrical laws and is very straightforward. It doesn't involve complex calculations nor spatial discretization of the environment. In a certain way the simplicity of this model fits the geometric simplicity of an RC.

1) Description of the initial source: The nature of the emitting source placed in the rectangular cavity must be defined properly. Since antenna type and shape have little influence on the statistical observation in an RC with a stirrer (as long as the antenna is properly placed in the RC), we choose not to describe the antenna precisely. In our model the emitting antenna is described by an elementary current that radiates the electromagnetic field. However this elementary current may have a particular position, an angular orientation (that defines its polarization) and a radiation pattern as described in II-B4. Therefore every image of this current constructed by the geometric laws of reflections is a current itself with the same radiation pattern but a particular position and a particular angular orientation.

2) Image creation: A rectangular cavity is a 3D resonator, its frequency response is dictated by its three dimensions (l, w, h) by the well-known resonant frequency formula:

$$f_{m,n,p} = \frac{c}{2}\sqrt{\left(\frac{l}{m}\right)^2 + \left(\frac{w}{n})\right)^2 + \left(\frac{h}{p}\right)^2} \qquad (1)$$

The reflections on the conductive walls create interferences and construct the frequency response of the cavity. By creating secondary sources (images), IT reproduces the reflection phenomenon. The idea is to simulate hundreds of reflections on the walls in order to construct a realistic frequency response. The first step is to create and determine the exact position and the exact orientation of every elementary image current. Their positions and orientations are a function of the dimensions of the rectangular cavity and the position (x_0, y_0, z_0) and orientation (tilt and azimuth angles α_0 and β_0) of the elementary current placed initially in the RC. Figure 1 shows the position of the image currents in the different image cavities. The initial cavity (order 0) is in bold line. The angular orientation of the image currents is determined by applying the construction rules presented in figure 2. The creation of the image current in the model is relatively straightforward. The number of image cavities for a given order $n > 0$ is given by:

$$C_n = 4n^2 + 2 \qquad (2)$$

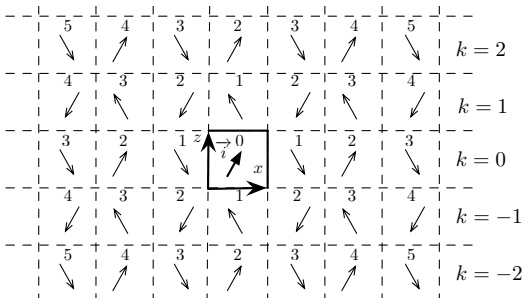

Fig. 1. Construction of the image currents (plane $y = y_0$). The initial cavity is in bold line.

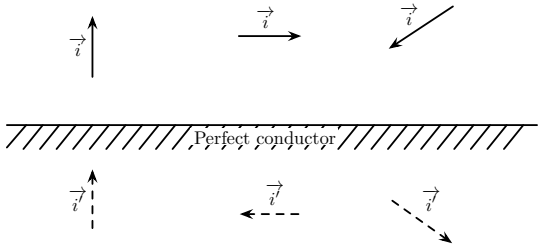

Fig. 2. Image theory and currents.

and the number of elementary currents M_n after n reflections is given by:

$$M_n = \sum_{i=0}^{n} C_i = 1 + 2n + \frac{2n(n+1)(2n+1)}{3}. \qquad (3)$$

3) Loss simulation: IT is presented with perfectly conductive materials. A real reverberation chamber is made of conductive materials and cavity loss is simulated by introducing three loss coefficients R_x, R_y, R_z corresponding to the three pairs of conducting walls of our cavity. If the conductive properties of the three pairs of walls are the same, we can assume that $R_x = R_y = R_z = R$ but we can imagine to simulate a less conductive wall or an opening by reducing one of the three coefficients. In this study the loss coefficient for each direction are equals. The *order* of an elementary image current cavity is the number of reflections involved in its creation. If we consider the elementary current a, created by i reflections along the Ox axis, j reflections along the Oy axis and k reflections along the Oz axis $(n = i + j + k)$, its intensity is given by:

$$I_a = I_0 R_x^i R_y^j R_z^k = I_0 R^n, \qquad (4)$$

with $R < 1$ and I_0 the intensity of the elementary current placed in the initial cavity (cavity of order 0). The total

amount of energy found in the system is proportional to:

$$\mathcal{E}_{tot} \propto I_0^2 + \sum_{i=1}^{\infty}(4i^2+2)I_0^2 \cdot R^{2i} \tag{5}$$

As $R < 1$ the energy contained in the system (cavity of order 0 and all the image cavities) converges when the number of reflections is infinite. More than a reflection coefficient, the coefficient R takes in account all the loss in the cavity (walls, lossy objects). The loss coefficient R in our model integrates roughly the absorption from lossy objects in the chamber. It can be seen as a time domain quality factor Q of the chamber considered constant over the bandwidth of the antennas and/or the pulse emitted to estimate the losses. The determination of R is done by measuring a channel impulse response (CIR) in the chamber and by simulating CIRs with different values of R. By computing the power delay profiles, we can find the value of the loss parameter R that matches the measurements. Measurements in our empty chamber have shown that with $R = 0.998$ the power delay profile curves are very similar. Values under 0.995 are generally chosen to simulate a loaded cavity. With $R = 0.97$ we can consider that the chamber is heavily loaded.

4) E-field calculation: When the position of every image current is determined and when the loss coefficient is estimated, the model computes the CIR by adding the contributions of all the currents in the system. The millions of image currents emit simultaneously an impulse. These impulses are collected at a chosen reception point in the real cavity (order 0). The E-field created by the elementary current a with a dipole radiation pattern ($\sin\theta$), a tilt angle α and an azimuth angle β can be written:

$$\overrightarrow{E_a}(t) = -\omega\mu\frac{dhI_0R^n f(t-t_a)}{4\pi d_a}\sin\theta_a \begin{cases} \cos\theta_a\cos\phi_a \cdot \overrightarrow{u} \\ \cos\theta_a\sin\phi_a \cdot \overrightarrow{v} \\ -\sin\theta_a \cdot \overrightarrow{w} \end{cases} \tag{6}$$

where dh is the length of the elementary current, ω is its pulsation, $f(t)$ is the impulsion emitted, t_a is the time of arrival to the reception point and d_a is the distance between the elementary current considered and the reception point. θ_a and ϕ_a are the angular coordinates of the reception point in the spherical system attached to the elementary current a. The basis $(\overrightarrow{u}, \overrightarrow{v}, \overrightarrow{w})$ is given by the following system:

$$\begin{cases} \overrightarrow{u} = \mathcal{R}_{\alpha,\beta} \cdot \overrightarrow{e_x} \\ \overrightarrow{v} = \mathcal{R}_{\alpha,\beta} \cdot \overrightarrow{e_y} \\ \overrightarrow{w} = \mathcal{R}_{\alpha,\beta} \cdot \overrightarrow{e_z} \end{cases}, \tag{7}$$

where $\mathcal{R}_{\alpha,\beta}$ is the rotation matrix that transform the rectangular coordinates system attached to the reverberation chamber into the rectangular coordinates system attached to the considered elementary current. $\mathcal{R}_{\alpha,\beta}$ represents a rotation of an angle α around a unitary vector $\overrightarrow{e_\beta} = -\cos\beta\overrightarrow{e_x} + \sin\beta\overrightarrow{e_y}$,

$$\mathcal{R}_{\alpha,\beta} = \begin{pmatrix} \cos^2\beta+(1-\cos^2\beta)\cos\alpha & -\cos\beta\sin\beta(1-\cos\alpha) & \sin\beta\sin\alpha \\ -\cos\beta\sin\beta(1-\cos\alpha) & \sin^2\beta+(1-\sin^2\beta)\cos\alpha & \cos\beta\sin\alpha \\ -\sin\beta\sin\alpha & -\cos\beta\sin\alpha & \cos\alpha \end{pmatrix}. \tag{8}$$

From the E-field expression (6) in the local rectangular coordinate system attached to the elementary current, we can deduce the expression in the rectangular coordinate system attached to the simulated cavity:

$$\overrightarrow{E}_{a_{(\overrightarrow{e_x},\overrightarrow{e_y},\overrightarrow{e_z})}} = \mathcal{R}^{-1}_{\alpha,\beta} \cdot \overrightarrow{E}_{a_{(\overrightarrow{u},\overrightarrow{v},\overrightarrow{w})}}. \tag{9}$$

The channel impulse response is given by adding the contribution of every current in our system. If M is the total number of currents in our system, from (6) we can deduce three channel impulse responses corresponding to the three rectangular components:

$$s_{x,y,z}(t) = \sum_{i=0}^{M} \overrightarrow{E_i}(t) \cdot \overrightarrow{e_{x,y,z}}. \tag{10}$$

The Fourier transform of the CIRs gives three frequency responses:

$$\mathcal{F}_{x,y,z}(f) = \text{FFT}(s_{x,y,z}(t)) \tag{11}$$

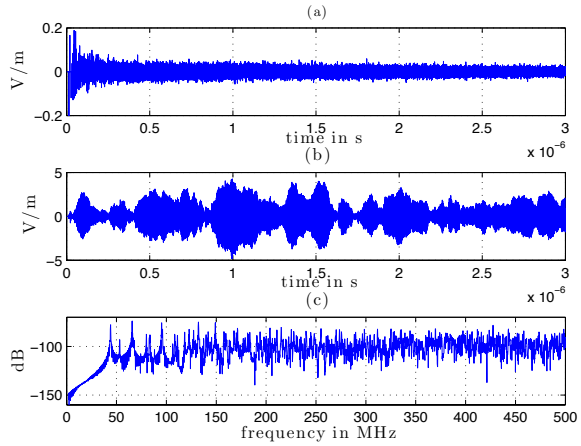

Fig. 3. E_z component: (a) Channel impulse response, (b) Response for a 300 ns long pulse at 1 GHz, (c) Frequency response.

C. Preliminary Results

In this section we present some results in the time domain and the frequency domain. Figure 3-(a) shows the CIR along the vertical component (E_z) obtained by our model with $R = 0.998$ at an arbitrary reception point in the initial cavity. We can note that the pulse amplitude is slowly decreasing. One can imagine that the power

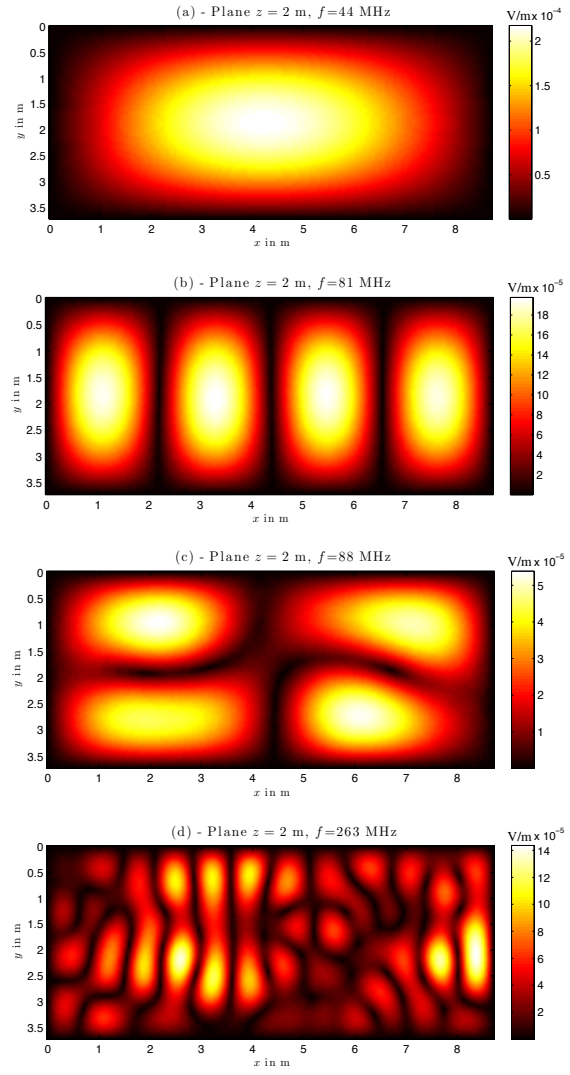

Fig. 4. E_z component of the electric field (linear values) in the plane $z = 2$ m at different frequencies. Various cavity modes: (a) TE_{110}, (b) TE_{410}, (c) TE_{220} and a combination of different cavity modes (d).

delay profile of such a configuration would be very long. After a convolution of this signal with a 300 ns long pulse at 1 GHz, we obtain the response of the cavity for this signal (fig. 3-(b)). Figure 3-(c) shows the frequency response of the channel obtained by applying a Fourier transform on the CIR. The frequency response clearly exhibits the resonant frequencies one should expect for a cavity of these dimensions ($8.7 \times 3.7 \times 2.9$ m). After 400 MHz, the Fourier transform exhibits fast fading.

In order to visualize the cavity modes involved for a given frequency and to verify that the physics of resonant cavities is respected, we performed simulations into a full horizontal plane of the cavity. Figure 4 shows the result obtained in a full plane after a Fourier transform of the vertical component (E_z). These results show clearly that the modes excited at a given frequency match the modes theoretically present in the cavity [6]. The geometry of the modes is respected and the boundary conditions that state that the tangential components of the E-field are null on the conductive walls are respected.

D. Effect of the length of the channel impulse response

The model presented in this article computes the first instants of the CIR. On a 64 bits system with 32 GB of memory, we are able to simulate the first 3 μs of the CIR. Low noise measurements have shown that a full CIR in our reverberation chamber is around 30 μs long when the cavity is empty. From the viewpoint of the amount of energy simulated, if we compute the cumulated power of the CIR measured in our RC, we can note that after 3 μs, 60% of the energy is simulated (fig. 5). The length of the CIR simulated affects the frequency response. When the CIR is very short, the fast Fourier transform of the CIR widens the modes. When the CIR is longer, the widening is less pronounced. The effect of this widening is accentuated at lower frequencies. As a result, the modes are artificially combined when the CIR is relatively short and it seems that the quality factor is lower. Figure 6 shows the effect of the length of the CIR on the statistics obtained for rectangular components of the E-field through the Anderson-Darling (AD) goodness of fit test (GoF) (presented in III-A1). We can notice that the Rayleigh distribution is largely accepted after 400 MHz when the CIR is only 500 ns long. Measurements have shown (in III-A1) that the Rayleigh distribution is largely accepted only after 900 MHz with these tests. With 2 or 3 μs long CIRs, the simulations fit the measurements (fig. 7). If the cavity is loaded with lossy elements, the CIR is shorter and we can expect to simulate a full CIR within the 3 μs. In order to show that a time window of 3 μs is enough to get relevant results, the next section compares the simulations and measurements in the worst case scenario, when the cavity is empty. The results in the next section show that with only 3 μs, the results obtained in the frequency domain are very accurate and follow the measurements greatly.

III. Frequency Domain Simulation of a Reverberation Chamber

A. Statistical analysis of the distribution of the rectangular components of the E-field

In this section, the model is used to simulate the behavior in the frequency domain of the RC of our laboratory without loading. In a real reverberation chamber, the rotation of the mode stirrer gives the statistic of the E-field. The implementation of a mechanical

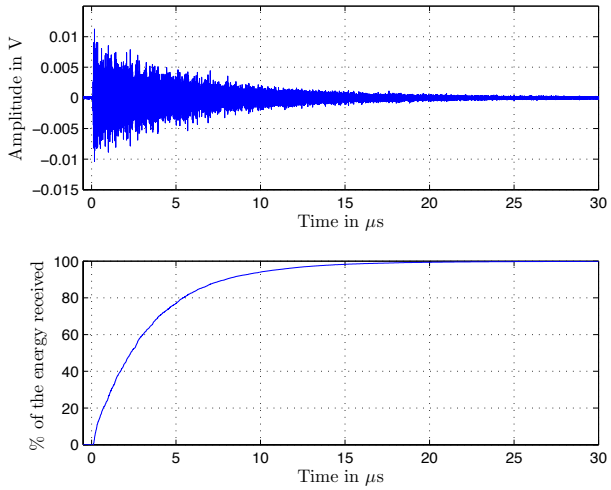

Fig. 5. Measured channel impulse response in the empty RC and percentage of the total energy of the impulse response vs. time

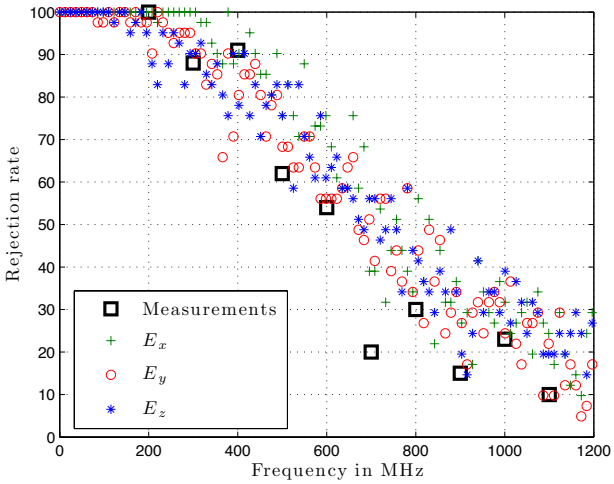

Fig. 7. Rejection rate in % with AD GoF test for the Rayleigh distribution with $N = 100$ vs. frequency. Results from E-field measurements and from simulations with $R = 0.998$.

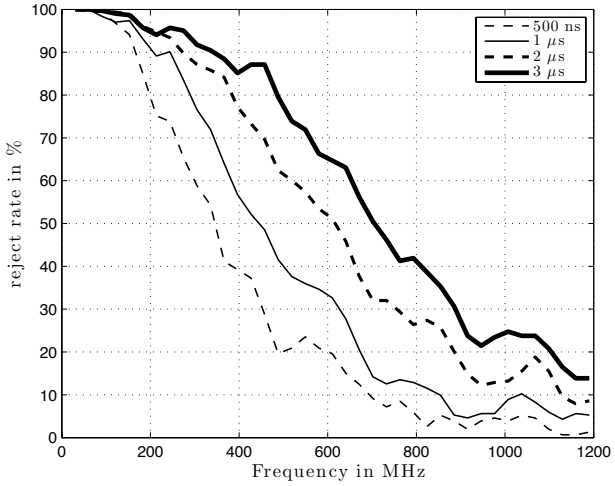

Fig. 6. Reject rate with the AD GoF test for the Rayleigh distribution for rectangular components of the E-field with $N = 150$ for different length of CIR, and an empy cavity ($R = 0.998$).

stirrer in our model is not easy, we choose another approach to create a statistic of the E-field. We collect data at different independent reception points [9]. This method is based on the ergodicity of the RC. We choose randomly N receiver positions and we verify that the distance between each point is greater than half the wavelength. The ergodicity of the RC states that by choosing N independent receiver positions, our approach is supposed to be equivalent to collecting data from N independent stirrer positions. The results are analyzed statistically and compared with measurements lead in the real chamber.

1) Statistical test for the Rayleigh distribution: With N independent positions, we compute N CIRs. The fast Fourier transform of these CIRs give a N size sample for every independent frequency [10]. Every sample is tested with the AD GoF test for Rayleigh distribution [11] with Stephen's values. The null hypothesis H_0 is accepted when the sample follows a Rayleigh distribution. On the contrary the alternative hypothesis H_1 favors that the distribution is not Rayleigh distributed. The level of significance $\alpha = 0.05$ means that the test will fail to recognize 5% percent of the Rayleigh distributions. This analysis gives the statistical behavior of the chamber as a function of the frequency. The results obtained with our model are compared with measurements made in our RC [11] with an electric field with an electric field probe (Hi6005) over 30 probe positions and at least 30 stirrer positions. Fig. 7 shows the rejection rate of the AD GoF statistical test for different frequencies for a measured rectangular component and for three rectangular components simulated in an empty cavity ($R = 0.998$) . These results show that the frequency domain behavior of our simulated cavity fits the behavior of our real RC. Measurements and simulated data are very similar. Our model is able to predict the statistic of a rectangular component of the E-field.

2) Statisitcal test for the Weibull distribution: If the behavior for frequencies above 600 MHz is clear (the Rayleigh assumption is massively accepted by the test), the behavior for frequencies under 600 MHz can be finely studied by using Weibull distributions [11], [12], [13]. For frequencies above the lowest usable frequency (LUF), the ideal model of the RC [1] is verified. For

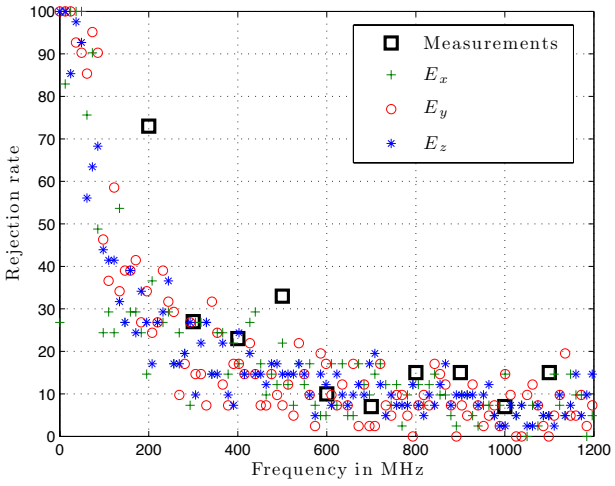

Fig. 8. Rejection rate in % with AD GoF test for the Weibull distribution with $N = 150$ vs. frequency. Results from E-field measurements and from simulations with $R = 0.998$.

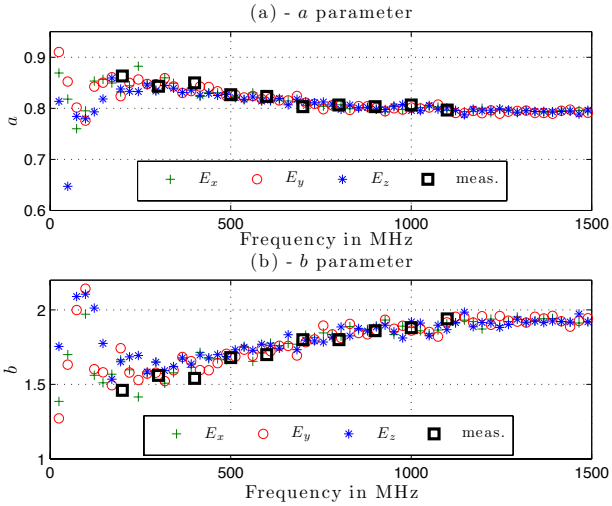

Fig. 9. Scale parameter a and shape parameter b from measurements and simulations vs. frequency.

low frequencies to frequencies around the LUF, Weibull distributions can be used to model the behavior of the RC. The probability density function of a Weibull random variable x is given by:

$$f(x; a, b) = abx^{b-1}e^{-ax^b} \text{ with } x \geq 0. \qquad (12)$$

Fig. 8 shows that around the LUF ($\approx$ 250MHz) and above, the AD GoF test for Weibull distribution is widely accepted. Here again simulated data and measurements are very similar.

3) Analysis of Weibull parameters: Each sample is divided by its mean value. If we study carefully the scale parameter a and the shape parameter b of the Weibull distribution [13] as a function of the frequency, we can note that the parameter a converges to a value around under 0.8 and that the parameter b converges to 2 when the frequency increases (fig. 9). Theoretically, with $a = \pi/4$ and $b = 2$, the Weibull distribution becomes a Rayleigh distribution. We can note that the values of the parameters a and b from the measurements and the simulations are almost identical and that the distribution of each component of the electric field tends to become a Rayleigh distribution when the frequency increases. These results show that the model developed is able to explore the frequency domain without a complete CIR simulation. It means that the amount of energy simulated is enough to perform a comprehensive study in the frequency domain with an empty cavity.

TABLE I
MEAN VALUES OF THE E-FIELD COMPONENTS MEASURED IN OUR RC

Frequency in MHz	E_x (V/m)	E_y (V/m)	E_z (V/m)
300	38.8	40.2	59.8
500	37.1	37.3	50.9
700	32.3	32.2	44.3
900	44.5	44.5	52.6
1100	15.3	15.2	18.3

B. Effect of the chamber dimensions on the rectangular components of the E-field.

The dimensions of the RC at the IETR are $8.7 \times 3.7 \times 2.9$ m. Measurements of the electric field with an electric field probe (Hi6005) over 30 probe positions and at least 30 stirrer positions in this chamber have shown an imbalance of the three rectangular components of the E-field. The mean value of the vertical component (E_z) is greater than the two other components (Tab. I). Our assumption is that our chamber is particularly long, the length (8.7 m) is more than twice the width (3.7 m) and the first cavity modes establish the E-field along the vertical components before the two other components. Globally the energy along the vertical component is greater than the two other components at low frequencies. When the frequency increases however, the mode density is greater and the difference between the components of the E-field is reduced. The model developed is used to verify this assumption. First we simulate our reverberation chamber, the emitting elementary current is oriented along the

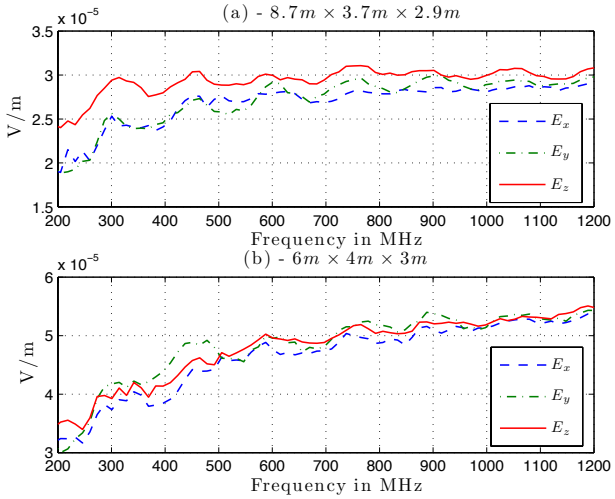

Fig. 10. Smoothed frequency response for the chamber of our laboratory (a) and a more conventional reverberation chamber (b)

vector $(1,1,1)$ (tilt angle and $\alpha = \pi/2 - \arccos(\sqrt{2/3})$ and azimuth angle $\beta = \pi/4$) in order to not favor any component, the number of simulations is 300. The result are smoothed over a large number of frequencies in order to show the general trend of each component. Figure 10-(a) shows that even if the loss in the chamber is not a function of the frequency, the simulation is in agreement with the measurements, the vertical component is greater than the two other components, but the difference is reduced when the frequency increases. A chamber whose dimensions are more common ($6 \times 4 \times 3$ m) is simulated. Figure 10-(b) shows that the components of the mean values of the E-field components with this chamber are more homogeneous.

IV. Conclusion

Even if the IT model developed was initially thought as a time domain model, the results presented in this article in the frequency domain show that this model is able to explore and understand the physics of the chamber in the frequency domain. With few physical elements (dimensions of the cavity, loss, position of the emitting antenna), this model reproduce with accuracy the statistical behavior of an RC in the frequency domain. The simulation of a mechanical stirrer is planned and may give an alternate stirring solution for the simulations. This very straightforward model may be helpful to simulate and optimize experiments with RC and may allow to understand the impact of various physical parameters on the electric fields in an RC.

Acknowledgement

This work was supported by the French Ministry of Defense DGA (Direction Générale de l'Armement) with a Ph.D grant delivered to Emmanuel Amador.

References

[1] D. Hill, "Plane wave integral representation for fields in reverberation chambers," *IEEE Transactions on Electromagnetic Compatibility*, vol. 40, no. 3, pp. 209–217, Aug 1998.

[2] A. Coates, H. Sasse, D. Coleby, A. Duffy, and A. Orlandi, "Validation of a three-dimensional transmission line matrix (TLM) model implementation of a mode-stirred reverberation chamber," *Electromagnetic Compatibility, IEEE Transactions on*, vol. 49, no. 4, pp. 734–744, Nov. 2007.

[3] C. Bruns and R. Vahldieck, "A closer look at reverberation chambers - 3-D simulation and experimental verification," *Electromagnetic Compatibility, IEEE Transactions on*, vol. 47, no. 3, pp. 612–626, Aug. 2005.

[4] M. Hoïjer, A.-M. Andersson, O. Lunden, and M. Backstrom, "Numerical simulations as a tool for optimizing the geometrical design of reverberation chambers," in *Electromagnetic Compatibility, 2000. IEEE International Symposium on*, vol. 1, 2000, pp. 1–6.

[5] G. Orjubin, F. Petit, E. Richalot, S. Mengue, and O. Picon, "Cavity losses modeling using lossless FDTD method," *Electromagnetic Compatibility, IEEE Transactions on*, vol. 48, no. 2, pp. 429–431, May 2006.

[6] R. Harrington, *Time-Harmonic Electromagnetic Fields*. New York: McGraw-Hill Book Company, 1961.

[7] D.-H. Kwon, R. Burkholder, and P. Pathak, "Ray analysis of electromagnetic field build-up and quality factor of electrically large shielded enclosures," *Electromagnetic Compatibility, IEEE Transactions on*, vol. 40, no. 1, pp. 19–26, Feb 1998.

[8] S. Baranowski, D. Lecointe, M. Cauterman, and B. Demoulin, "Use of 2D models to characterize some features of a mode stirred reverberation chamber," vol. 9-13. International Symposium on Electromagnetic Compatibility, Sorrento, Italy, september 2002, pp. 381–386.

[9] D. Hill and J. Ladbury, "Spatial-correlation functions of fields and energy density in a reverberation chamber," *Electromagnetic Compatibility, IEEE Transactions on*, vol. 44, no. 1, pp. 95–101, Feb 2002.

[10] C. Lemoine, P. Besnier, and M. Drissi, "Estimating the effective sample size to select independent measurements in a reverberation chamber," *Electromagnetic Compatibility, IEEE Transactions on*, vol. 50, no. 2, pp. 227–236, May 2008.

[11] ——, "Investigation of reverberation chamber measurements through high-power goodness-of-fit tests," *Electromagnetic Compatibility, IEEE Transactions on*, vol. 49, no. 4, pp. 745–755, Nov. 2007.

[12] ——, "Proposition of tolerance requirements adapted for the calibration of a reverberation chamber," in *Electromagnetic Compatibility, 2009 20th International Zurich Symposium on*, Jan. 2009, pp. 41–44.

[13] A. Papoulis, *Probability, Random Variables, and Stochastic Processes*, 4th ed. New York: Mc Graw Hill, 2002.